IMAGING THE ALTERATION AND DEFORMATION HALO ABOVE THE DIORITE-TONALITE INTRUSIVE AT THE NGATAMARIKI GEOTHERMAL FIELD.

Steve Sewell[1], Martha Savage[1], John Townend[1], Chet Hopp[1], Stefan Mrocek[1] and Kenny Graham[1]

[1] School of Geography, Environment and Earth Sciences, Victoria University, Wellington, NEW ZEALAND, 6140

Steven.Sewell83@gmail.com

Keywords: *Ngatamariki, Rotokawa, seismic tomography*

ABSTRACT

An expanded seismic array of ~55 seismometers deployed across the Rotokawa and Ngatamariki geothermal fields during 2017 and 2018 was used to derive 3D seismic velocity models via local earthquake tomography using P and S wave traveltimes from a set of 302 microseismic events. These events were mostly from three clusters of seismic activity around injection wells within the fields. The P and S arrival times used in the inversions were from both manual picking (90 events) and high-quality automatic picking (261 events) with estimated arrival times accurate to approximately ± 0.05 s for P and ± 0.1 s for S. The tomography code tomoDD was used for the inversions that progressed from 2D to coarse to fine inversion grids in order to examine the improvement in traveltime residuals with increasing model discretization. A 1D constant-velocity starting model previously determined using Monte Carlo VELEST was used for most models. In addition to this, a further fine inversion grid was constructed with a 3D starting velocity model based on available well-logging data (checkshot and sonic logs) and geological information. Model solution robustness and spatial resolution were assessed using derivative weight sum (DWS) values that provide a measure of ray-path coverage in conjunction with synthetic recovery tests (spike test and interpretation model test). The inversion models strongly indicate that a west to east, high to low-velocity variation of at least ±10% Vp and Vs exists across northern Ngatamariki. The high velocity in the west is interpreted to be due predominantly to the very low porosity that formed within the Tahorakuri Formation due to high temperature alteration and ductile deformation during intrusion of a diorite-tonalite magma approximately 600 thousand years ago. The location of the transition from high to low velocity agrees well with a transition from high to low gravity from the publicly available gravity data in the area and a transition from high to low resistivity from a 3D inversion of magnetotelluric (MT) data. Relatively low Vp and Vs is imaged in the east of Ngatamariki and is most likely due to either a greater proportion of porous volcaniclastics and sediments and less rhyolite lava in the upper 1 km and/or deeper smectite and smectite-illite clay alteration in that area, as suggested by magnetotelluric data. High Vs is observed at Rotokawa, which is interpreted as being due to the shallower contacts of the andesite and greywacke. An alternative explanation is that there is less volcaniclastics/sediments and more rhyolite lava in the upper 1 km. Since the magmatic alteration and deformation in the north of Ngatamariki is associated with low-permeability wells, the tomography results can be used to inform future well targeting and numerical modelling of the field.

1. INTRODUCTION

1.1 The Ngatamariki and Rotokawa Geothermal Fields

The Ngatamariki and Rotokawa Geothermal fields are high-temperature geothermal fields in the Taupo Volcanic Zone in the central North Island of New Zealand (Figure 1). Electricity generation on the Rotokawa field began in 1997 with a small binary power plant (34 MWe) and in 2010 a second 138 MWe triple flash power plant was installed, bringing the total installed field capacity to 172 MWe. A microseismic monitoring array of 10 seismometers has been operating at Rotokawa since mid-2008. Production on the Ngatamariki field began in 2013 with the commissioning of an 83 MWe binary plant. Nearly 100% of the produced fluid at Ngatamariki is injected in two locations, ~1.5 km north and south of production wells (Figure 1). A microseismic monitoring network has operated at Ngatamariki since mid-2012 that consists of nine surface seismometers and three downhole seismometers installed in monitoring wells between 300-500m depth.

1.2 Seismic velocity in geothermal fields

Seismic velocity is known to vary with respect to important geothermal reservoir properties such as porosity/permeability, temperature and water/steam saturation (e.g. Boitnott, 1995; Jaya et al., 2010) and therefore techniques that provide images of seismic velocity have potential application to geothermal resource well targeting, monitoring and management. Seismic tomography is one such technique that can provide seismic velocity images of the subsurface, commonly using P and S wave arrival times from local earthquakes (e.g. Rawlinson and Sambridge, 2003). Although no field-scale, seismic tomography work has been published for the Ngatamariki and Rotokawa geothermal fields, a number of seismic velocity variations are expected within the fields based on geological variations and seismic velocity logging data (Sewell et al. 2021 *this volume*). The northern part of Ngatamariki is known to be low permeability (NM4 and NM8 starting injectivities < 1 t/h.bar and conductive temperature profiles) due to the presence of an old intrusive body and its associated alteration halo (Chambefort et al., 2016). Using measured velocities at Ngatamariki from wireline sonic logs in NM8, NM9 and NM10, Sewell et al. 2021 *this volume* have shown that the Tahorakuri Formation tuffs and volcaniclastics above the intrusive in the north of the field (NM8 and NM9) have significantly lower porosity (approximately 10% lower) and consequently higher Vp (approximately 0.5-1 km/s faster) than the same formation in the south of the field (NM10). They relate this to both quartz-deposition infilling pore space and ductile deformation and closure of pore space several hundred metres directly above the intrusive where temperatures in the past have been above the brittle-ductile transition (>350°C, Violay et al. (2017)). Sherburn et al., (2003) reported a high-Vp anomaly (>15% above background) in the north of Ngatamariki that they attributed

ISSN 2703-4275

to the intrusive body. However, this feature was not well resolved spatially as the study used a regional seismic monitoring network with wide spacing between seismometers. As the intrusion and its alteration is associated with low permeability, imaging the high velocity with tomography may allow future wells drilled at Ngatamariki to be targeted away from this low permeability area.

The primary purpose of this study was to investigate the 3D velocity structure of the Ngatamariki and Rotokawa fields using local earthquake tomography. To do this, a dense array of 50 seismometers was deployed across the two fields for a one-year period between 2017 and 2018 with the aim of improving the spatial resolution of velocity variations within the field (Figure 1).

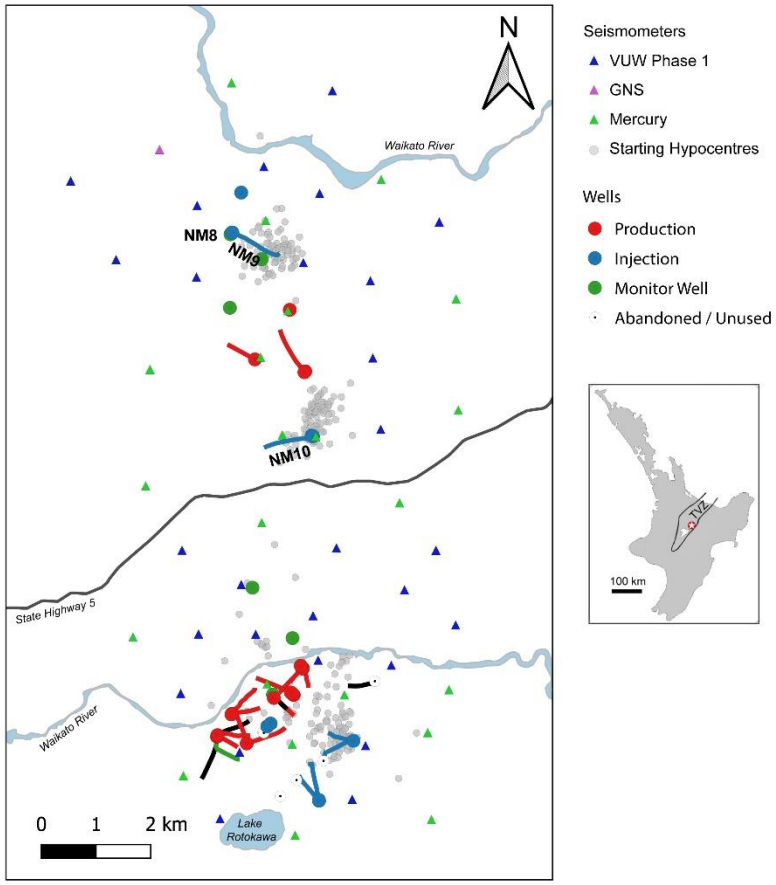

Figure 1. The Ngatamariki (north of State Highway 5) and Rotokawa (south of State Highway 5) geothermal fields. Triangles show the location of seismometers and grey dots show the starting hypocentres locations used in this work.

2. DATA AND METHODS

2.1 Travel-time dataset

The travel-time data used consisted of both manually picked and automatically picked P and S wave arrival times from 302 earthquakes mostly from the three main clusters of activity (Rotokawa, Ngatamariki South and Ngatamariki North) near injection areas in the geothermal fields. 100 well-recorded events (those with >30 P picks and >10 S picks) were initially selected from a catalog of automatically located hypocentres that were then manually re-picked. These events were distributed across the study area with an emphasis on selecting events that occurred outside of the three main clusters of microseismic activity. The manual picking followed the procedure of Diehl and Kissling, (2009) and included manually picking arrival time uncertainties. This showed that 90% of the manually picked arrival uncertainties were within ±0.04 s for P arrivals and were within ±0.09 s for S arrivals. In total, P and S picks were available for 63 stations, or 61 if excluding stations with <10 picks (SS32 and SS35).

The manual picking resulted in a catalog with more events at Rotokawa than at Ngatamariki South and Ngatamariki North as manually reviewed events for Ngatamariki South and Ngatamariki North were often found to be of poorer quality (as they are lower magnitude than events at Rotokawa). To obtain an approximately even distribution of events for each of the main clusters and to increase the total number of picks, automatically picked events were added to the catalog. The automatically picked events were selected based on having at least 10 P and 1 S picks with high pick SNR. Comparison of results using only the manual picks and the manual and automatic picks showed little difference in the final velocity models, station corrections and RMS residuals for each model which indicates that there was no significant increase in the amount of pick noise by adding the automatic picks. The final catalog used consisted of 302 events with 6778 P arrivals and 2436 S arrivals.

The Python program hypoDDpy (Krischer, 2015), which uses the Obspy framework (Beyreuther et al., 2010), was used to generate the differential traveltime data. Catalog differential times were generated for all event pairs within 1 km of each other (effectively

linking most event pairs within each of the three main clusters of seismicity - northern Ngatamariki, southern Ngatamariki and Rotokawa). Cross-correlation differential times were also generated for all phase and event pairs within 1 km of each other, however only cross-correlation differential times for event pairs within 0.5 km of each other were used in the inversions. In total, 111,858 catalog P, 19,972 catalog S, 61,533 cross-correlation P and 10,928 cross-correlation S traveltimes were generated.

2.2 Seismic Velocity Inversion

The program tomoDD (Zhang, 2003) was used to invert both absolute and differential traveltime data to obtain Vp and Vs models. The inclusion of differential traveltime data in the inversion has been shown to sharpen velocity contrasts within and surrounding the clusters of seismicity for which the differential data are calculated (Zhang, 2003). The large-scale velocity structure is however dominantly determined by the absolute traveltime data. Velocity model parameterization is via a grid of nodes with tri-linear interpolation of velocity between the nodes to obtain a continuous velocity media. Inversion is via the LSQR damped least-squares algorithm and both damping and smoothing regularization are used to stabilize the inversion and obtain a model that is close to the starting model and minimizes the velocity model complexity required to fit the traveltime data down to the noise level. Three data types are able to be used in tomoDD – absolute traveltimes, catalog differential times and cross-correlation traveltimes. These are implemented in the inversion in a hierarchical scheme whereby each data type is weighted differently throughout the inversion.

To investigate the velocity model complexity that is required to obtain an adequate fit to the absolute data, inversions were first performed using only the absolute data with six different model parameterizations with increasing complexity from a 2D grid through to a fine grid with 1 km node spacings (Figure 2). For all of these inversions, nodes with derivative weight sum values (a measure of ray path coverage e.g. Thurber and Eberhart-Phillips, (1999)), less than 0.1 times the average of all nodes were fixed in the inversion, thereby preventing nodes that are not sampled by the ray paths from changing. Damping only was used in the 1D and 2D inversions whereas both damping and smoothing were used in the coarse and fine 3D models. In each of the 3D models, an L-curve test was performed to obtain appropriate values for the damping and smoothing values. Inversions for the absolute data were run for 5 iterations of hypocentre only followed by 5 iterations of joint hypocentre-velocity. The change in residual RMS between the 4^{th} and 5^{th} and 9^{th} and 10^{th} iterations was small for all inversions (approximately <5 ms RMS), showing that the hypocentre and velocity model solutions had converged.

To make use of available a priori velocity information and to test sensitivity of the final model to the starting velocity model, a 3D starting velocity model (referred to as the 'geo' model) was developed based on the checkshot survey, well-logging data and geological information. In this starting model, both the northwest corner of Ngatamariki and the Rotokawa area were given higher starting velocities (Figure 2). For northwest Ngatamariki, the starting velocities approximate those obtained from the checkshot survey and Vp log in NM9. For the Rotokawa area, higher starting velocities between 1 km bsl and 2 km bsl approximate those obtained for andesite and greywacke from sonic logs (Vp and Vs for andesite in NM10) and seismic refraction survey velocities of Stern and Benson, (2011) for greywacke. The starting model hence accounts for the difference in elevation of the top of andesite between Ngatamariki and Rotokawa (approximately 2 km bsl for Ngatamariki (Chambefort et al., 2014) versus approximately 1-1.5 km bsl for Rotokawa (McNamara et al., 2016)). Everywhere else in the 3D geo starting model the starting values were as per the 1D starting model. In all starting models, the Vp/Vs ratio was set to be 1.8 based on the average obtained from the dipole sonic logs in NM8 and NM10.

2.3 Synthetic testing

Synthetic testing was performed to assess how well resolved the velocity models were. Based on the recommendations of Rawlinson and Spakman, (2016), spike testing was performed rather than a checkboard resolution test. This was done to better assess smearing of velocity onto nodes that are relatively unconstrained by the available ray paths, particularly above 1 km bsl. Synthetic arrival times were generated through a velocity model consisting of velocity spikes 1 × 1 × 1 km in size and ±10 % velocity variation from the 1D starting velocity. The spikes were separated by one node in east-west and two nodes in north-south and were placed between 1.5 and 2.5 kmbsl. The synthetic arrivals were then inverted using the same parameters as were used in the inversion of the real data. Synthetic recovery tests of the main interpreted velocity structures were also performed to assess how well resolved spatially these features are. All synthetic tests were performed both with and without randomly generated Gaussian pick noise with a standard deviation of 0.05 s for P and 0.1 s for S, which was based on the standard deviation of the manually picked uncertainties.

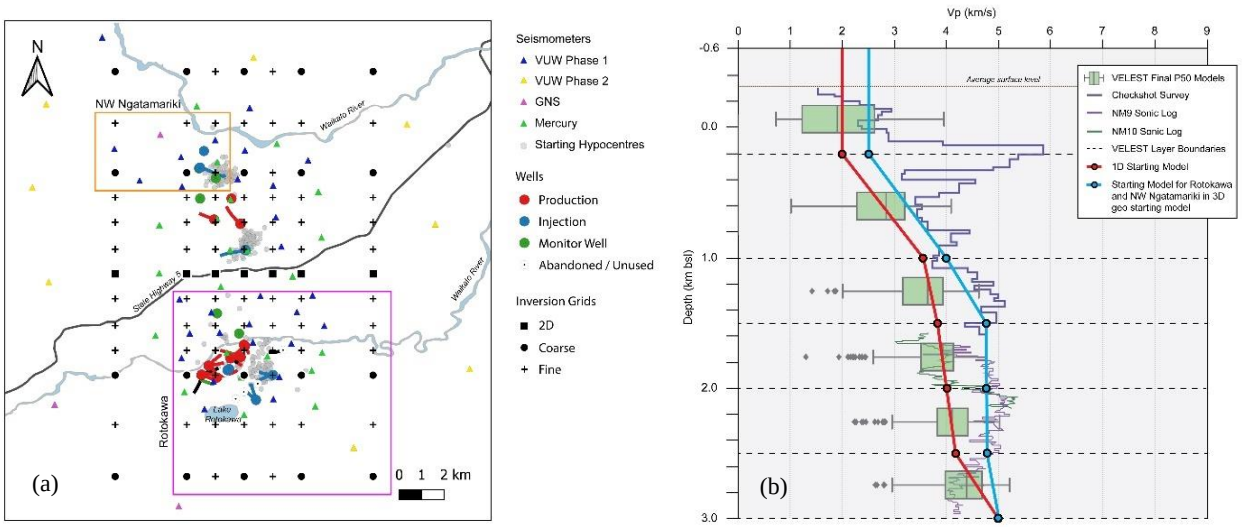

Figure 2. (a) The inversion grid nodes. The orange rectangle shows the location of nodes that were assigned higher starting velocity in the 'geo' starting model. (b) The 1D starting velocity model (red) based on results from a monte-carlo VELEST analysis (box and whisker plots) and the velocity used in NW Ngatamariki (orange box in (a)) and Rotokawa (pink bow in (a)) in the 3D 'geo' starting model.

3. RESULTS

3.1 Data fit

1D and 2D velocity models were not able to fit the data to the level of noise (approximately ± 0.05s for P and ± 0.1s for S) (Table 1). All of the 3D velocity models (coarse, fine and geo models) provided an adequate fit to the data. The coarse model provides a reasonably good fit to both the P and S data, with most residuals less than ±0.1 s for P and less than ±0.2 s for S. The fine and geo models show improvement in residual fit relative to the coarse model, however the improvement is smaller than when moving from the 2D to the coarse model. The fine and geo models both fit the P and S residuals close to the expected level of uncertainty in the pick data. The difference in data fit between the fine and geo model is relatively minor with the fine model obtaining a slightly better fit to the data than the geo model. The catalog and cross-correlation differentials for the double difference runs were well fit with RMS residuals of 61 ms for catalog and 25 ms for cross-correlation data for the fine model and 73 ms for catalog and 16 ms for cross-correlation in the geo model.

Table 1. Mean and standard deviation (std) of traveltime residuals for the different model parameterizations.

Model	P residual mean (ms)	P residual std (ms)	S residual mean (ms)	S residual std (ms)
1D	2	82	-139	252
2D	4	72	-66	228
Coarse	6	59	-4	158
Fine	6	52	-21	130
Geo	6	56	31	141

3.2 Data Coverage

Derviative weight sum values (DWS) values, a measure of ray-path coverage (Thurber & Eberhart-Phillips, 1999), for Vp and Vs clearly show that the area between the earthquake clusters and between 1 to 2 km bsl has the best ray-path coverage. The highest DWS values were obtained at 1.5 and 2 km depths for both P and S waves with values of >1000 for P and >100 for S in an area extending between the main earthquake clusters. Events at southern Ngatamariki and Rotokawa are larger magnitude than those for northern Ngatamariki and are therefore better recorded across the array. This is likely the reason for very high DWS in the south between RK and NM south at 2 km depth. DWS values at 1 km bsl are approximately half those at 1.5 and 2 km for the area between earthquakes (~500 for P, ~50 for S). Relatively low DWS values for 0.2 km bsl is due to ray paths at this depth travelling mostly vertically and therefore the average length of ray travelling close to each node is low. DWS values are low for 2.5 and 3 km depth as the earthquakes are mostly at or above these depths. The DWS values agree well with the results of the synthetic testing that further show that depths between 1.0 and 2.0 km bsl are best resolved for this dataset and that there is poor constraint at 0.2, 2.5 and 3 km bsl (see Synthetic Testing below).

3.3 Velocity models

All four non-1D models (2D, coarse, fine and geo) had a west to east, high to low variation in Vp and Vs across northern Ngatamariki between 0.2 and 2 km depth. The transition between high to low velocity in all cases occurred approximately through the middle of the Ngatamariki field with the transition being sharper in the fine and geo models. Since the 'geo' model incorporated a more realistic starting model based on the measured velocities in logs and the known geological variation in the two fields, the preferred velocity model presented here is the 'geo' model. The 'fine' and 'geo' models however had very similar spatial patterns with the main differences being the absolute values of the velocity, demonstrating that the starting model does not result in significantly different interpretations. Depth slices for the geo model over the best constrained are shown in Figure 3.

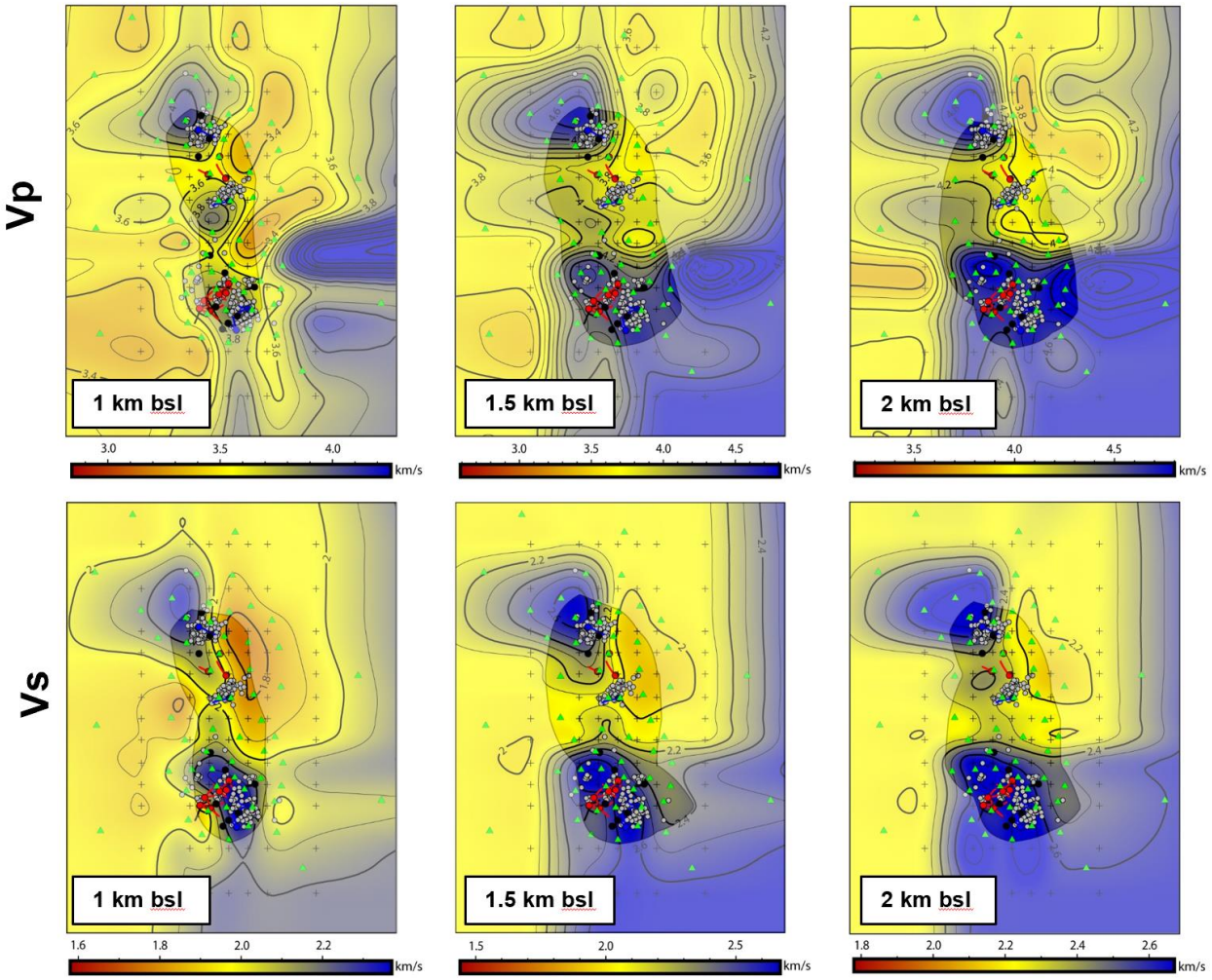

Figure 3. Vp (upper panel) and Vs (lower panel) for the 'geo' model. The area with good ray coverage (P DWS > 500, S DWS > 50) is fully transparent. Green triangles show the station locations, grey dots the earthquakes. The color scale ranges between ± 10% of the 1D starting velocity model.

3.4. Synthetic testing

The best recovery for the spike test for both Vp and Vs was at 1.5 km bsl with reasonable recovery also obtained for 2 km bsl. At both of these depths, and for both Vp and Vs, the region encompassing the earthquakes was best recovered, with both the shape of velocity variations and whether the velocity was relatively high or low being generally recovered. The recovery of the shape of the velocity variations is slightly worse with the addition of pick noise to the synthetic data. Recovery directly adjacent to the area between the hypocentres but still within the dense array is partially recovered for Vp at 1.5 and 2 km bsl but not for Vs. This likely reflects the overall lower amount of S wave data as shown by the lower DWS values for Vs relative to Vp. Areas outside of the dense array and at 2.5 km bsl were poorly recovered due to the lack of ray coverage. Velocity variations were introduced by the inversion at 0.2 and 1.0 km bsl despite the synthetic model having the same constant velocity as the starting model for the inversion. These variations became more prominent with the addition of pick noise to the synthetic data. In all cases, the magnitude of the velocity values were underestimated by the inversion. For the best recovered area between the earthquakes at 1.5 km bsl, the percent difference in velocity between the synthetic model and the recovered model is approximately ±50% (i.e. the recovered velocity values are approximately half those of the synthetic model). Recovery of the true velocity values was poorer for 2 km bsl.

4. DISCUSSION

A high to low, west to east velocity variation is consistently observed across northern Ngatamariki for both Vp and Vs between 0.2 and 2 km bsl in all of the 3D models (coarse, fine and geo) (Figure 3). Consistent with expectations based on well logs (Sewell et al., 2021 *this volume*), high velocity (Vp and Vs) in NW Ngatamariki is likely due to the alteration and deformation that occurred within the Tahorakuri Formation during the emplacement of the diorite-tonalite intrusive. As discussed by Sewell et al., 2021 *this volume* the logging data for NM9 in the north and NM10 in the south show a difference in Vp on the order of 1 km/s for the Tahorakuri Formation which was shown to be due to a porosity difference on the order of 10-15% between north and south. The high velocity is unlikely to be directly due to the intrusive itself as the DWS and synthetic testing both show that the dataset used here is relatively insensitive to velocity variations at the depth of the intrusive (below 2 km bsl). It is possible that some of the high velocity may be due to higher velocity within the upper 1 km related to thicker rhyolite lavas that outcrop in the northwest.

The transition from high velocity in the west to low velocity in the east across northern Ngatamariki was consistently placed across the NM9 well in all models (2D, coarse, fine and geo). This suggests that NM9 may be close to the edge of the intrusive body and its alteration and deformation halo. The location of the transition is coincident with transitions seen in the available gravity data and MT resistivity at 1.5 kmbsl (Figure 4 and Figure 5). Both the high gravity and high resistivity in the northwest are likely related to the same low porosity Tahorakuri Formation above the intrusive. The west-east transition from high to low velocity was well recovered in the interpretation model synthetic testing between 1.0 and 2.0 km bsl and the spike test showed good recovery in the area of the transition for both Vp and Vs. Therefore, the high to low transition should be relatively well resolved (on the order of± 1 km) in the east-west direction by the available traveltime data.

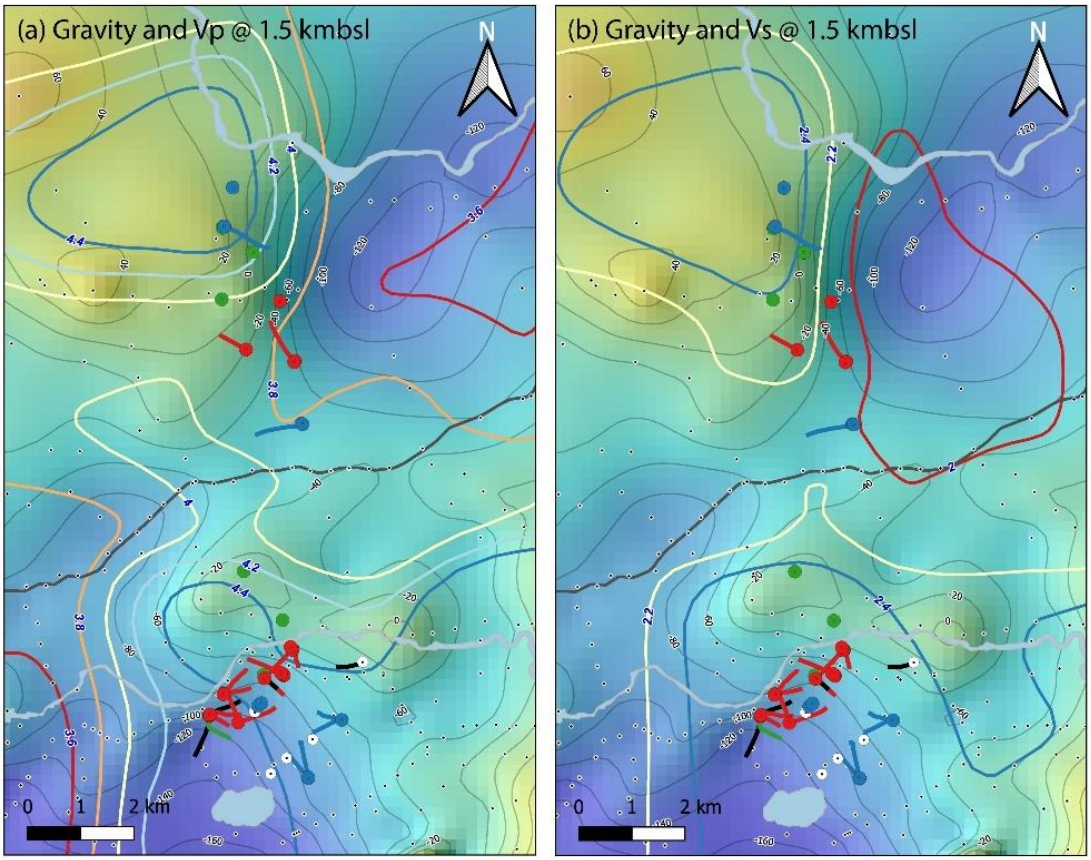

Figure 4. Comparison between seismic velocity and gravity data. (a) Contours of Vp at 1.5 km bsl from the geo model overlain on Bouguer gravity (mGal). (b) Contours of Vs at 1.5 km bsl from the geo model overlain on Bouguer gravity. Black circles with white outlines show the location of gravity stations.

Low velocity (Vp and Vs) in the east of Ngatamariki occurs between 0.2-2 km bsl (Figure 3). One explanation for the low-velocity to the east of Ngatamariki is the deepening of smectite and smectite-illite alteration within the Tahorakuri Formation. Wells drilled at Ngatamariki show that the Tahorakuri Formation in the south of the field (NM7-NM5-NM6) is smectite and smectite-illite altered to depths of up to 1.5 km bsl. MT surveys conducted at Ngatamariki image this alteration (Boseley et al., 2010) as a thick conductive layer that deepens to the east and southeast of the field (Figure 5). Smectite and smectite-illite clays have been widely shown to lower seismic velocity relative to illite and chlorite clays (e.g. Eberhart-Phillips et al., 1989) and the deepening of the smectite and smectite-illite alteration to the east of Ngatamariki is one possible explanation for the low-velocity.

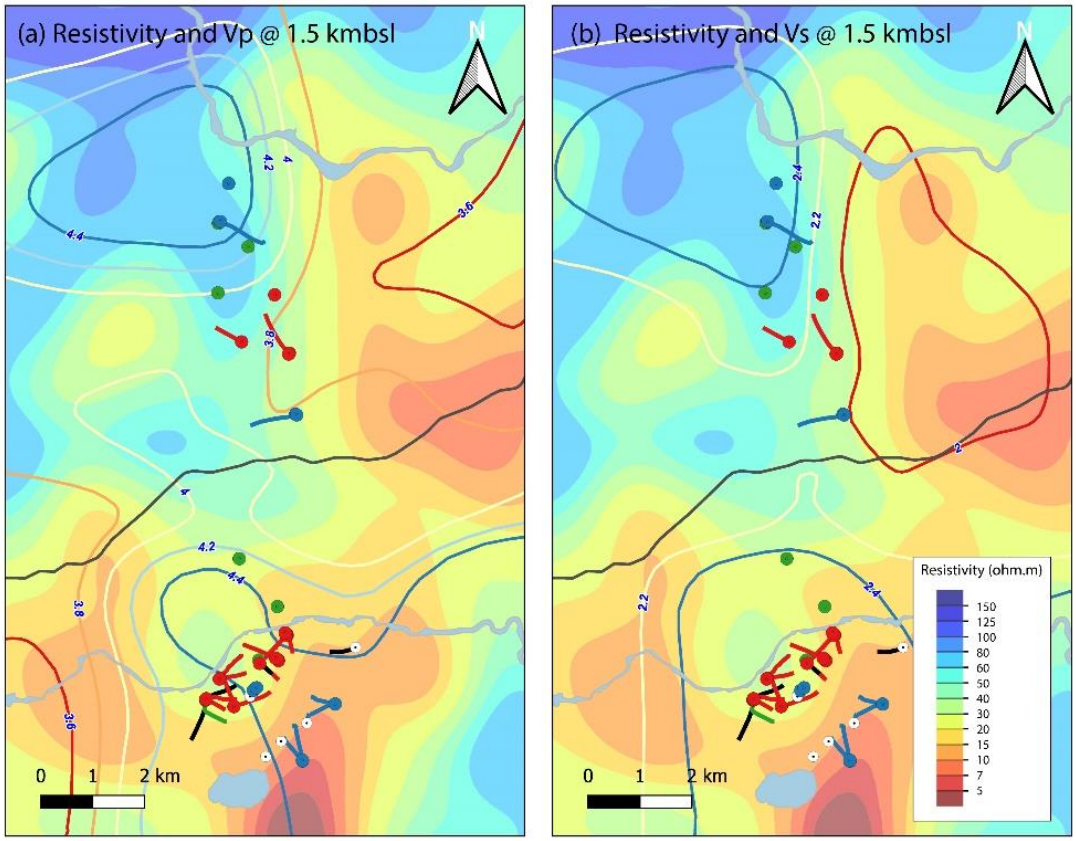

Figure 5. Comparison of resistivity at 1.5 km bsl from a 3D inversion of magnetotelluric data across the two fields and (a) Vp contours at 1.5 km bsl and (b) Vs at 1.5 km bsl from the geo model.

Gravity data also show a low to the east of Ngatamariki, however this is not well defined spatially due to the sparse station spacing (Figure 4). The gravity low is part of a broader low gravity region termed the 'Mihi' gravity low which Stagpoole et al. (2020) interpreted as possibly due to the Mihi Breccia, a pyroclastic flow unit interpreted to have formed during subaqueous rhyolite dome building (Downs, 2016). The Mihi low is part of a broader low gravity feature across the Taupō-Reporoa basin (Stagpoole et al., 2020). Given that the area east of Ngatamariki is more towards the axis of the Taupō-Reporoa Basin, it is also possible that some of the low velocity in this area can be attributed to a greater proportion of pyroclastics and sedimentary rocks and less rhyolite lava in the upper 1 km.

The high Vp and Vs at Rotokawa can be attributed to, at least in part, the higher elevation of the greywacke and andesite contacts relative to Ngatamriki (1 to 1.5 km bsl at Rotokawa versus 2 to 2.5 km bsl at Ngatamariki, Chambefort et al. (2014)). However, part of the high Vs (and likely Vp) at Rotokawa may also be due to the greater thicknesses of rhyolite lavas which outcrop to the north and northeast (McNamara et al., 2016).

The imaging of the transition from high velocity to low velocity across northern Ngatamariki in this study suggests that the low porosity and permeability Tahorakuri formation above the intrusive does not extend to the east and northeast of the current northern injection wells at Ngatamariki. Therefore, future wells in the field targeted to the east and northeast of the current northern injection wells would be less likely to encounter low permeability. Ideally the velocity transition would be better defined spatially by active source methods (e.g. checkshot/VSP with sensors in inactive wells in the north of the field and various offsets from those wells to the east) prior to drilling in this area. A more detailed gravity survey may also assist in further defining the transition from low porosity / high density Tahorakuri Formation above the intrusive to higher porosity / lower density Tahorakuri Formation away from the instrusive.

5. CONCLUSION

This study has shown that at least three large-scale 3D velocity variations exist across the Rotokawa and Ngatamariki fields. High velocity (Vp and Vs) is evident for northwest Ngatamariki from 0.2 to 2.0 km bsl which possibly extends to the southwest of the field. This is associated, at least in part, with the very low porosity and low permeability Tahorakuri Formation that was highly altered and ductily deformed during emplacement of the Ngatamariki diorite-tonalite intrusive. That the high velocity does not extend to the northeast of Ngatamariki suggests that the low permeability encountered in NM8 and NM4 does not extend to the northeast and future wells in the field might be targeted in this area. High velocity (Vs and most likely Vp) is observed at Rotokawa that is likely due, at least in part, to the shallower contact of andesite/greywacke at Rotokawa relative to Ngatamariki. A higher proportion of rhyolite lava and less volcaniclastics and sediments in the upper 1 km is another possible contributing factor.

ACKNOWLEDGEMENTS

The authors wish to acknowledge the Rotokawa Joint Venture (Mercury Energy and Tahaura North No. 2) for providing the seismic data and facilitating the field work, particularly David Wooton.

REFERENCES

Beyreuther, M., Barsch, R., Krischer, L., Megies, T., Behr, Y., & Wassermann, J. (2010). ObsPy: A Python Toolbox for Seismology. *Seismological Research Letters*, *81*(3).

Boitnott, G. N. (1995). *Laboratory measurements on reservoir rocks from the Geysers Geothermal Field*.

Boseley, C., Cumming, W., Urzúa-Monsalve, L., Powell, T., & Grant, M. (2010). A resource conceptual model for the Ngatamariki geothermal field based on recent exploration well drilling and 3D MT resistivity imaging. *Proceedings World Geothermal Congress*.

Chambefort, I., Buscarlet, E., Wallis, I., Sewell, S., & Wilmarth, M. (2016). Ngatamariki Geothermal Field, New Zealand: Geology, geophysics, chemistry and conceptual model. *Geothermics*, *59*, *Part B*, 266–280. https://doi.org/http://dx.doi.org/10.1016/j.geothermics.2015.07.011

Chambefort, I., Lewis, B., Wilson, C. J. N., Rae, A. J., Coutts, C., Bignall, G., & Ireland, T. R. (2014). Stratigraphy and structure of the Ngatamariki geothermal system from new zircon U–Pb geochronology: Implications for Taupo Volcanic Zone evolution. *Journal of Volcanology and Geothermal Research*, *274*, 51–70. https://doi.org/10.1016/j.jvolgeores.2014.01.015

Diehl, T., & Kissling, E. (2009). *Users Guide for Consistent Phase Picking at Local to Regional Scales*.

Downs, D. T. (2016). Mihi Breccia: A stack of lacustrine sediments and subaqueous pyroclastic flows within the Taupo Volcanic Zone, New Zealand. *Journal of Volcanology and Geothermal Research*, *327*, 180–191. https://doi.org/10.1016/j.jvolgeores.2016.08.004

Eberhart-Phillips, D., Han, D.-H., & Zoback, M. D. (1989). Empirical relationships among seismic velocity, effective pressure, porosity, and clay content in sandstone. *GEOPHYSICS*, *54*(1), 82–89. https://doi.org/10.1190/1.1442580

Jaya, M. S., Shapiro, S. A., Kristinsdóttir, L. H., Milsch, H., & Spangenberg, E. (2010). Temperature dependence of seismic properties in geothermal rocks at reservoir conditions. *Geothermics*, *39*(1), 115–123. https://doi.org/10.1016/j.geothermics.2009.12.002

Krischer, L. (2015). *hypoDDpy* (No. 1). https://github.com/krischer/hypoDDpy

McNamara, D., Sewell, S., Buscarlet, E., & Wallis, I. (2016). A review of the Rotokawa geothermal field, New Zealand. *Geothermics*. http://www.sciencedirect.com/science/article/pii/S0375650515000905

Rawlinson, N., & Sambridge, M. (2003). Seismic traveltime tomography of the crust and lithosphere. *Advances in Geophysics*, *46*, 81–199.

Rawlinson, N., & Spakman, W. (2016). On the use of sensitivity tests in seismic tomography. *Geophysical Journal International*, *205*(2). https://doi.org/10.1093/gji/ggw084

Sewell, S., Simpson, M., Gazeley, M., & Savage, M. (2021). Geophysical, geochemical and mineralogical characteristics of the alteration and deformation halo above the diorite-tonalite intrusive at Ngatamariki. *Proc. NZ Geothermal Workshop 2021*.

Sherburn, S., Bannister, S., & Bibby, H. (2003). Seismic velocity structure of the central Taupo Volcanic Zone, New Zealand, from local earthquake tomography. *Journal of Volcanology and Geothermal Research*, *122*(1–2), 69–88. https://doi.org/10.1016/S0377-0273(02)00470-5

Stagpoole, V., Miller, C., Caratori Tontini, F., Brakenrig, T., & Macdonald, N. (2020). A two million-year history of rifting and caldera volcanism imprinted in new gravity anomaly compilation of the Taupō Volcanic Zone, New Zealand. *New Zealand Journal of Geology and Geophysics*, 1–14. https://doi.org/10.1080/00288306.2020.1848882

Stern, T., & Benson, A. (2011). Wide-angle seismic imaging beneath an andesitic arc: Central North Island, New Zealand. *Journal of Geophysical Research: Solid Earth*, *116*(9). https://doi.org/10.1029/2011JB008337

Thurber, C., & Ritsema, J. (2007). Theory and Observations – Seismic Tomography and Inverse Methods. In *Treatise on Geophysics* (pp. 323–360). Elsevier. https://doi.org/10.1016/B978-044452748-6.00009-2

Thurber, Clifford, & Eberhart-Phillips, D. (1999). Local earthquake tomography with flexible gridding. *Computers & Geosciences*, *25*(7), 809–818. https://doi.org/10.1016/S0098-3004(99)00007-2

Violay, M., Heap, M. J., Acosta, M., & Madonna, C. (2017). Porosity evolution at the brittle-ductile transition in the continental crust: Implications for deep hydro-geothermal circulation. *Scientific Reports*, *7*(1), 7705. https://doi.org/10.1038/s41598-017-08108-5

Zhang, H. (2003). *Double-difference seismic tomography method and its applications*.